DALTON
FULL PAPER

Synthesis and characterization of dinuclear complexes containing the Fe^{III}–F · · · $(H_2O)M^{II}$ motif

Morten Ghiladi,[a] Kenneth B. Jensen,[a] Jianzhong Jiang,[b] Christine J. McKenzie,*[a] Steen Mørup,[b] Inger Søtofte[c] and Jens Ulstrup[c]

[a] *Department of Chemistry, University of Southern Denmark, Main campus: Odense University, DK-5230 Odense M, Denmark. E-mail: chk@chem.sdu.dk*
[b] *Department of Physics, Technical University of Denmark, Building 307, DK-2800 Lyngby, Denmark*
[c] *Department of Chemistry, Technical University of Denmark, Building 207, DK-2800 Lyngby, Denmark*

Received 6th April 1999, Accepted 23rd June 1999

The dinucleating phenolate-hinged ligand 4-*tert*-butyl-2,6-bis[bis(2-pyridylmethyl)aminomethyl]phenolate ($bpbp^-$) has been used to prepare a series of $Fe^{III}M^{II}$ complexes containing independent species at the exogenous binding sites. These sites are occupied by fluoride and water ligands and show the general formulation $[(bpbp)Fe(F)_2M(H_2O)_n][BF_4]_2$, M = Zn or Cu, $n = 1$; M = Co or Fe, $n = 2$. Two terminal fluoride ions are bound to the iron(III) ion and one or two water ligands to the adjacent divalent metal ion. The fluoride ligands are derived from the hydrolysis of tetrafluoroborate. In the crystal structure of $[(bpbp)Fe(F)_2Cu(H_2O)][BF_4]_2·4H_2O$. The copper(II) and iron(III) atoms are linked asymmetrically by the phenolic oxygen atom hinge of $bpbp^-$ with Cu–$O_{phenolato}$ 2.270(2) and Fe–$O_{phenolato}$ 2.041(2) Å with a Cu · · · Fe distance of 3.828(1) Å. The two terminal fluoride ions are bound to the Fe atom (Fe–F 1.818(2), 1.902(2) Å) and one of them is strongly hydrogen bonded to the water molecule on the adjacent Cu atom (F–H · · · O 2.653(4) Å). The metal ions in the aquafluoride complexes $[(bpbp)Fe(F)_2M(H_2O)_2][BF_4]_2$, M = Fe or Co, are weakly antiferromagnetically coupled ($J = -8$ and -10 cm^{-1} respectively) and in $[(bpbp)Fe(F)_2Cu(H_2O)][BF_4]_2$ are weakly ferromagnetically coupled ($J = 2$ cm^{-1}). The spectroscopic, electrochemical and magnetic properties of these complexes are compared to those of an analogous series of complexes containing two acetate bridging groups in the exogenous site. Electrochemical results indicate that the iron(III) ions in the bis-fluoride complexes are stabilized by about 300 mV towards reduction compared to the bis-μ-acetate complexes. The crystal structure of one bis-μ-acetate complex, $[Fe_2(bpbp)(CH_3CO_2)_2][BF_4]_2$, shows the expected arrangement; the iron-(II) and -(III) atoms are triply bridged by the phenolic oxygen atom of $bpbp^-$ and two μ-acetate groups with Fe^{II}–$O_{phenolato}$ 2.088(4) and Fe^{III}–$O_{phenolato}$ 1.951(5) Å and an Fe · · · Fe distance of 3.380(2) Å. The crystal structure at 120 K indicates that the iron atoms are valence trapped and in accordance with this Mössbauer measurements between 80 and 200 K show clearly distinguishable iron-(II) and -(III) components. The Mössbauer spectra of $[(bpbp)Fe(F)_2Cu(H_2O)][BF_4]_2·4H_2O$ are influenced by paramagnetic relaxation effects with relaxation times of the order of 1 ns. The relaxation time increases when a magnetic field is applied. This effect can be explained by a model for cross-relaxation in conjunction with the crystal symmetry of the compound.

Introduction

Mixed-valence diiron and dimanganese and heterometallic complexes using acyclic phenolate-hinged ligands with two chemically identical metal binding compartments are well known, and with few exceptions[1,2] they contain bridging exogenous ligands, usually oxo-acids or tetrahedral oxoanions.[3] The present article describes a continuation of our work on the isolation and characterization of mixed-valence and heterodimetallic complexes of 4-*tert*-butyl-2,6-bis[bis(2-pyridylmethyl)aminomethyl]phenolate ($bpbp^-$) in which the remaining metal co-ordination sites are occupied by terminal ligands. The compounds here contain the $[(bpbp)Fe^{III}F_2M^{II}]^{2+}$ core, where M = Fe, Cu, Co or Zn. The fluoride ions are bound as terminal ligands to the iron(III) atoms and water(s) are co-ordinated as terminal ligands to the divalent metal ions. These systems are rare examples of dimetallic complexes in which the endogenous ligand furnishes the only group linking the two metal ions; the species bound at the exogenous sites are independent (Fig. 1). One of these compounds, $[(bpbp)Fe(F)_2Fe(H_2O)_2][BF_4]_2·4H_2O$, was reported earlier,[2] and a poor quality crystal structure was obtained; unfortunately doubt remained as to the location of hydrogen atoms, and indeed as to the nature of the mononegative terminal ligands (fluoride or hydroxide ions). The characterization of analogous mixed metal complexes here now supports this original formulation.

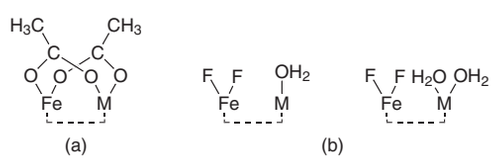

Fig. 1 Core structures based on $[(bpbp)Fe^{III}M^{II}]^{2+}$: (a) triply bridged bis-μ-acetato and (b) singly bridged difluoroaqua structures (the phenolate-hinged dinucleating ligand, $bpbp^-$, is represented by dashed lines).

Apart from the binary metal fluorides, only two structurally characterized iron co-ordination compounds containing the fluoride ion as a terminal ligand are known.[4] In contrast to the systems described here these are iron(III) porphyrin complexes. The preparation of transition metal complexes containing terminal fluoride ligands is not trivial since addition of F^- ions to a reaction mixture seldom leads to the pure fluoro complex. This obstacle has been overcome by using anhydrous metal fluorides as starting materials in suitable solvents.[5] Fluoride-containing transition metal complexes have been obtained also through partial decomposition of polyfluorinated counter ions,

a synthetic strategy which is based on the work of Musgrave and Linn.[6] Using this method Reedijk and co-workers[7] have prepared copper and cobalt complexes of azole ligands containing fluoride as bridging moieties. We have found in the present work that the preparation of complexes containing the Fe–F···(H$_2$O)M moiety can also be accomplished using this method.

Heterodimetallic Fe/M or mixed-valence diiron complexes containing the fluoride ligands are relevant structural models for fluoride-inhibited purple acid phosphatases (PAPs). To date no structural data using single crystal methods or EXAFS to analyse fluoride inhibited PAPs have been reported. Crowder and co-workers[8] have carried out kinetic and EPR studies of the reaction of bovine spleen PAP with an excess of fluoride, however the number of fluoride ions co-ordinated to the active site was not ascertained. The crystal structure of red kidney bean PAP without substrate or inhibitor at the dimetallic active site has been solved and the distance between the iron(III) and zinc(II) ions refined to 3.26 Å.[9] Consistent with this distance, and apart from the endogenous protein-derived bridging aspartate oxygen atom, a bridging exogenous hydroxide ion was assigned on the basis of the spectroscopic and kinetic studies. In the fluoride inhibited PAP it has been anticipated that a fluoride ion can replace co-ordinated hydroxide ion. Thus the characterization of iron(III)/metal(II) complexes with bridging and/or terminal fluoride ions is pertinent in establishing possible F^- ion inhibition modes in the PAPs.

Experimental

Dry acetonitrile and dry MeOH were obtained from Sigma-Aldrich Chemical Company, Inc. (>99.8%) and used as received. The UV/VIS spectra were recorded on a Shimadzu UV-3100 spectrophotometer, IR spectra of the complexes in KBr discs using an Hitachi 270-30 IR spectrometer, fast atom bombardment mass spectra on a Kratos MS50RF spectrometer and ^{19}F NMR spectra were recorded on a Varian Gemini 2000 using α,α,α-trifluorotoluene as an internal reference. Elemental analyses were performed at the Chemistry Department II at Copenhagen University and Atlantic Microlab, Inc., Norcross, Georgia, USA. Fluoride analyses were carried out by Dr J. Theiner, Institut für Physikalische Chemie der Universität Wien, Mikroanalytisches Laboratorium, A-1090 Vienna, Austria. Cyclic voltammograms were recorded using an Eco Chemie Autolab potentiostat equipped with an ECD low-current auxiliary module and controlled by the General Purpose Electrochemical Systems v.3.2 software (Eco Chemie software). The all-glass cell consisted of a working and a reference compartment connected *via* a Luggin capillary. The working compartment contained a platinum disc (5 mm in diameter) working electrode and a semi-cylindrical platinum gauze auxiliary electrode. The reference compartment contained a silver wire reference electrode immersed in a 0.01 M $AgNO_3$ solution in dry solvents separated from the bulk solution by a porous Vycor plug. Dry acetonitrile, methanol or 20% v/v acetone in CH_2Cl_2 solutions, with 0.1 M tetrabutylammonium perchlorate as the supporting electrolyte, were used. For measurements in acetone–CH_2Cl_2 solutions the reference electrode contained dry acetonitrile. Ambient temperature and an N_2 atmosphere were used throughout. The ferrocenium–ferrocene couple was used to check the reference electrode potential in acetonitrile, methanol and 20% v/v solution of acetone in CH_2Cl_2 and was found to occur at 89, −175 and 200 mV, respectively. Magnetic susceptibility measurements were performed by the Faraday method in the temperature range 78–300 K at a field strength of 1.3 T using instrumentation described elsewhere.[10] The variation of susceptibility with temperature can be described reasonably well by the equations derived from the Heisenberg–Dirac–Van Vleck model for isotropic binuclear magnetic exchange interactions ($H = -2J\cdot S_1\cdot S_2$).[11] The J values are estimated to be accurate to within 20%. The molar susceptibility was corrected for underlying diamagnetism by the use of Pascal's constants. Mössbauer spectra were obtained with a conventional Mössbauer spectrometer in the constant acceleration mode using a 50 mCi source of ^{57}Co in Rh. The calibration was performed using a 12.5 μm thick foil of α-Fe at room temperature, relative to which all isomer shifts are given. The spectra were computer fitted using a least squares procedure.

The preparations of 4-*tert*-butyl-2,6-bis[bis(2-pyridylmethyl)-aminomethyl]phenol (Hbpbp), [(bpbp)Fe(F)$_2$Fe(H$_2$O)$_2$][BF$_4$]$_2$·4H$_2$O and [(bpbp)FeM(CH$_3$CO$_2$)$_2$][ClO$_4$]$_2$ (M = Co, Ni, Cu, Zn or Fe) are described elsewhere.[2]

Preparations

[(bpbp)Fe(F)$_2$M(H$_2$O)$_n$][BF$_4$]$_2$, for M = Zn or Cu, n = 1; for M = Co, n = 2. A solution of Hbpbp (0.3000 g, 0.52 mmol) in 2 mL of acetone was added to a solution of Fe(BF$_4$)$_2$·6H$_2$O (0.1755 g, 0.52 mmol) in 10 mL water. One equivalent of the appropriate hydrated M(BF$_4$)$_2$ salt was then added. The products crystallized in *ca.* 95% yield within two days. Calc. for [(bpbp)Fe(F)$_2$Co(H$_2$O)$_2$][BF$_4$]$_2$·2.5H$_2$O, $C_{36}H_{48}B_2CoF_{10}FeN_6O_{5.5}$: C, 44.16; H, 4.94; F, 19.40; N, 8.58. Found: C, 44.13; H, 4.66; F, 19.91; N, 8.40%. FAB mass spectrum: *m*/*z* 724 (35, [(bpbp)FeCo(F)$_2$]$^+$) and 743 (28%, [(bpbp)FeCo(F)$_3$]$^+$). ^{19}F NMR (300 MHz): δ 8.9 (s) and 78.0 (s). UV-Vis (methanol): λ_{max}/nm (ε/dm^3 mol^{-1} cm^{-1}) 255 (14500), 295 (6800, sh) and 476 (650). Calc. for [(bpbp)Fe(F)$_2$Cu(H$_2$O)][BF$_4$]$_2$·4H$_2$O, $C_{36}H_{49}B_2CuF_{10}FeN_6O_6$: C, 43.55; H, 4.97; F, 19.14; N, 8.46. Found: C, 43.86; H, 4.60; F, 20.15; N, 8.37%. FAB mass spectrum: *m*/*z* 260 (100, [$C_{12}H_{11}N_3Cu$]$^+$), 709 (25, [(bpbp)FeCu(F)]$^+$), 728 (40, [(bpbp)FeCu(F)$_2$]$^+$) and 747 (33%, [(bpbp)FeCu(F)$_3$]$^+$). ^{19}F NMR (300 MHz): δ 4.0 (s) and 80.6 (s). UV-Vis (methanol): λ_{max}/nm (ε/dm^3 mol^{-1} cm^{-1}) 253 (15800, sh), 300 (7180, sh) and 494 (860). Calc. for [(bpbp)Fe(F)$_2$Zn(H$_2$O)][BF$_4$]$_2$·3.5H$_2$O, $C_{36}H_{48}N_6O_{5.5}B_2F_{10}FeZn$: C, 43.47; H, 4.97; F, 19.10; N, 8.45. Found: C, 44.01; H, 4.72; F, 18.75; N, 8.41%. FAB mass spectrum: *m*/*z* 729 (70, [(bpbp)FeZn(F)$_2$]$^+$) and 748 (75%, [(bpbp)FeZn(F)$_3$]$^+$). ^{19}F NMR (300 MHz): δ 5.8 (s) and 78.2 (s). UV-Vis (methanol): λ_{max}/nm (ε/dm^3 mol^{-1} cm^{-1}) 258 (13100), 295 (6020) and 472 (600).

[Fe$_2$(bpbp)(CH$_3$CO$_2$)$_2$][BF$_4$]$_2$. A solution of Hbpbp (0.0711 g, 0.124 mmol) in 1 mL of acetone was added to a solution Fe(BF$_4$)$_2$·6H$_2$O (0.0838 g, 0.248 mmol) in 1 mL water. Ethyl acetate was diffused into the mixture and dark blue crystals of the product deposited over several days in 70% yield. Calc. for [Fe$_2$(bpbp)(CH$_3$CO$_2$)$_2$][BF$_4$]$_2$, $C_{40}H_{45}B_2F_8Fe_2N_6O_5$: C, 49.27; H, 4.65; N, 7.18. Found: C, 49.36; H, 4.50; N, 7.27%. UV-Vis (CH$_3$CN): λ_{max}/nm (ε/dm^3 mol^{-1} cm^{-1}) 256 (21900), 296 (sh, 8440), 329 (sh, 5140), 381 (sh, 3000) and 555 (1040).

X-Ray crystallography

Crystals of [(bpbp)Fe(F)$_2$Cu(H$_2$O)][BF$_4$]$_2$·4H$_2$O and [Fe$_2$(bpbp)(CH$_3$CO$_2$)$_2$][BF$_4$]$_2$ were obtained directly from reaction mixtures. Table 1 contains the crystal data and details of the structural determinations. The crystals were cooled to 120 K using a Cryostream nitrogen gas cooler system.[12] The data were collected on a Siemens SMART Platform diffractometer with a CCD area sensitive detector. Three of the water molecules of [(bpbp)Fe(F)$_2$Cu(H$_2$O)][BF$_4$]$_2$·4H$_2$O are disordered. The non-hydrogen atoms were refined anisotropically. The hydrogen atoms of [(bpbp)Fe(F)$_2$Cu(H$_2$O)][BF$_4$]$_2$·4H$_2$O except for the disordered water molecules were located from electron-density difference maps and refined isotropically. The hydrogen atoms of the disordered water molecules were not included in the refinement. The hydrogen atoms of [Fe$_2$(bpbp)(CH$_3$CO$_2$)$_2$][BF$_4$]$_2$ were placed at calculated positions using a riding model with fixed thermal parameters [U(H) = 1.2U for attached atom].

Programs used for data collection, data reduction and absorption were SMART, SAINT and SADABS.[13] The program SHELXTL 95[14] was used to solve the structures and for molecular graphics; PLATON[15] was used for molecular geometry calculations.

CCDC reference number 186/1536.

See http://www.rsc.org/suppdata/dt/1999/2675/ for crystallographic files in .cif format.

Results and discussion

Syntheses

The dinuclear complexes $[(bpbp)Fe^{III}(F)_2M(H_2O)_n][BF_4]_2$, M = Zn or Cu, $n = 1$; M = Co or Fe,[2] $n = 2$, are prepared from a mixture of Hbpbp and one equivalent each of iron(II) tetrafluoroborate and the appropriate divalent metal tetrafluoroborate. The compounds crystallize in almost quantitative yields within two days at ambient temperature. The two fluoride ions bound to the iron(III) are derived from hydrolysis of the counter anion. Attempts to prepare the same series of complexes using fluoride salts or metal fluorides as the fluoride ion source did not result in tractable products. Interestingly diffusion of ethyl acetate into a 1:2 mixture of Hbpbp and iron tetrafluoroborate in acetone led to the precipitation of the bis-acetate-bridged complex, $[Fe_2(bpbp)(CH_3CO_2)_2][BF_4]_2$ rather than the bis fluoro complex $[(bpbp)Fe(F)_2Fe(H_2O)_2][BF_4]_2\cdot 4H_2O$ that is obtained in its absence. The acetate bridging groups are derived from the hydrolysis of ethyl acetate, thus hydrolysis rather than abstraction of fluoride from tetrafluoroborate is apparently favoured under these reaction conditions. The crystal structure of $[Fe_2(bpbp)(CH_3CO_2)_2][BF_4]_2$ was determined in order to verify the presence of two acetate bridges. The novel alternative of a combination of one acetate bridge and terminal fluoride, water or hydroxide ligands was considered a possibility given the unusual reaction conditions. The preparations of this bis-acetato-bridged complex and those we have previously reported with perchlorate counter anions[2] contrast markedly to the preparations of other similar acetate-bridged complexes for which the bridging groups are provided by acetate ion sources.[3]

Elemental analyses of the fluoride complexes have been fitted with extra water corroborating the proposal of one or two waters as ligands on the divalent metal ions. Water as lattice solvent is present also in all the complexes and confirmed in the crystal structures of $[(bpbp)Fe(F)_2Cu(H_2O)][BF_4]_2\cdot 4H_2O$ (Fig. 2) and $[(bpbp)Fe(F)_2Fe(H_2O)_2][BF_4]_2\cdot 4H_2O$.[2] It is not possible unequivocally to assign the number of water ligands in the complexes without crystal structures however a formulation has been made on the basis of expected geometrical similarities of the Fe/Fe (crystal structure) and Fe/Co and the Fe/Cu (crystal structure) and Fe/Zn complexes. Thus there is one terminal aqua ligand in the complexes containing Cu^{II} and Zn^{II}, and two aqua ligands in the complexes containing Fe^{II} and Co^{II}. Five- or six-co-ordination is feasible for the Zn atom in the non-crystallographically characterized Fe/Zn complexes, thus it is not possible to distinguish between the structural formulations of $[(bpbp)Fe(F)_2Zn(H_2O)]^{2+}$ or $[(bpbp)Fe(F)_2Zn(H_2O)_2]^{2+}$ for the cations in the Fe/Zn complexes in the absence of a crystal structure. A geometry close to that found for the copper containing analogue in Fig. 2 is considered as the most likely, hence the formulation given for the zinc complex. Crystals of the Fe/Co and the Fe/Zn complexes diffracted poorly and in attempts to obtain better crystals these complexes were isolated as perchlorate salts by using zinc or cobalt perchlorate in place of the tetrafluoroborate starting materials. The full characterization of these perchorate salts was not made since even though suitably sized crystals of $[(bpbp)Fe(F)_2Co(H_2O)_2][ClO_4]_2$ and $[(bpbp)Fe(F)_2Zn(H_2O)][ClO_4]_2$ were formed these also diffracted too weakly for crystal structure analysis.

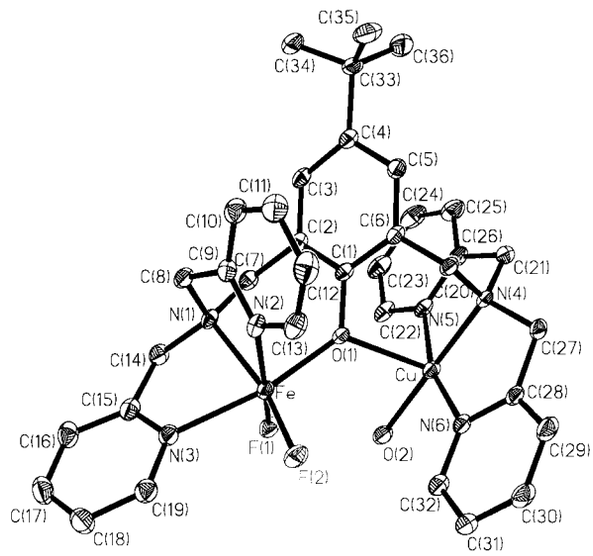

Fig. 2 The molecular arrangement of the cation in $[(bpbp)Fe(F)_2Cu(H_2O)][BF_4]_2\cdot 4H_2O$, showing 50% probability ellipsoids. The hydrogen atoms are omitted for clarity.

Establishing the presence of fluoride ligands (*e.g.* rather than OH^-) by elemental analysis was difficult in light of the presence of fluoride in the counter anions. However fluorine analyses combined with ^{19}F NMR spectroscopy confirm the presence of both co-ordinated fluoride and the fluoride of the counter anion. The signal for the co-ordinated fluoride ion at *ca.* δ 78 for all the complexes is broad and paramagnetically shifted. The FAB mass spectra of all the tetrafluoroborate complexes show intense peaks corresponding to the difluorinated cations $[(bpbp)FeM(F)_2]^+$. Ions containing three fluoride atoms were also observed; these may be assigned to the trifluorinated cations $[(bpbp)FeM(F)_3]^+$ or ion pairs $\{[(bpbp)FeM(F)_2]^{2+}[F]^-\}^+$ which may result from the gas phase decomposition of the counter anion. In no case is the water ligand(s) retained. The mass spectrometry results are consistent with the 100% formation of the mixed metal complexes; no signals that can be assigned to homodinuclear analogues are detected.

Crystal structure of $[(bpbp)Fe(F)_2Cu(H_2O)][BF_4]_2\cdot 4H_2O$

Selected bond distances and angles are listed in Table 2 (see Table 1 for other crystallographic parameters). The copper(II) and iron(III) atoms in $[(bpbp)Fe(F)_2Cu(H_2O)][BF_4]_2\cdot 4H_2O$ (Fig. 2) are bridged asymmetrically by the phenolic oxygen atom of $bpbp^-$ with Cu–O 2.270(2) and Fe–O 2.041(2) Å with a Cu···Fe distance of 3.828(1) Å. As support for the formulation, the refinement of this structure was clearly improved by using fluorine atoms rather than hydroxide oxygen atoms as the exogenous terminal ligands attached to Fe^{III} in the model. The two terminal fluoride ions are bound to the Fe atom and one of them, F1, is strongly hydrogen bonded to the water molecule on the adjacent Cu atom (F1···H–O 2.653(4) Å). The other fluoride ion is hydrogen bonded to the ordered water molecule (F2···H–O 2.688(4) Å). The hydrogen atoms of the water molecules were located on electron density difference maps. Hydrogen bonding probably stabilizes the terminal fluoride ligands. The geometries around the iron(III) and copper(II) are octahedral and square pyramidal respectively. The apical bond on the copper ion is that to the phenolate oxygen atom. As a result the complex is highly unsymmetrical with a difference of 0.14 Å between the Fe–O1 and the Cu–O1 bonds.

Notably, and similarly to terminal fluoride ligands, terminal hydroxide ligands are rarely characterized in the solid state in iron(III) complexes.[4,16] The crystal structure of $[(bpbp)Fe(F)_2Fe(H_2O)_2][BF_4]_2\cdot 4H_2O$ reported earlier was of extremely poor quality and the result ambiguous with regard to

Table 1 Crystallographic data

	$[(bpbp)Fe(F)_2Cu(H_2O)][BF_4]_2\cdot 4H_2O$	$[Fe_2(bpbp)(CH_3CO_2)_2][BF_4]_2$
Formula	$C_{36}H_{49}B_2CuF_{10}FeN_6O_6$	$C_{40}H_{45}B_2F_8Fe_2N_6O_5$
Formula weight	976.82	975.14
Crystal symmetry	Monoclinic	Monoclinic
Space group	$P2_1/c$	$P2_1/n$
a/Å	17.9414(8)	12.191(2)
b/Å	13.6413(6)	21.792(4)
c/Å	18.8617(9)	16.435(3)
β/Å	112.260(1)	93.92(3)
V/Å^3	4272.3(3)	4356.0(15)
Z	4	4
$\mu_{(MoK\alpha)}$/mm^{-1}	0.93	0.75
T/K	120	120
Total no. unique reflections	10844	8541
No. observed reflections [$I > 2\sigma(I)$]	7590	3941
R	0.0538 (obs.)	0.0850 (obs.)
$wR2$	0.1481 (all)	0.2144 (all)

Table 2 Selected bond lengths (Å) and angles (°) for the cation of $[(bpbp)Fe(F)_2Cu(H_2O)][BF_4]_2\cdot 4H_2O$

Fe–F2	1.818(2)	Cu–N6	1.967(3)
Fe–F1	1.902(2)	Cu–O2	2.024(2)
Fe–O1	2.041(2)	Cu–N5	2.025(3)
Fe–N1	2.112(3)	Cu–N4	2.070(3)
Fe–N2	2.149(3)	Cu–O1	2.270(2)
Fe–N3	2.234(3)		
F2–Fe–F1	100.20(9)	N1–Fe–N3	79.78(10)
F2–Fe–O1	106.01(9)	N2–Fe–N3	95.26(10)
F1–Fe–O1	90.15(9)	N6–Cu–O2	95.35(11)
F2–Fe–N1	162.81(10)	N6–Cu–N5	164.55(11)
F1–Fe–N1	89.99(9)	O2–Cu–N5	97.77(11)
O1–Fe–N1	87.62(9)	N6–Cu–N4	86.16(11)
F2–Fe–N2	91.24(10)	O2–Cu–N4	177.74(11)
F1–Fe–N2	168.43(9)	N5–Cu–N4	80.50(11)
O1–Fe–N2	84.94(10)	N6–Cu–O1	98.90(9)
N1–Fe–N2	79.36(10)	O2–Cu–O1	87.55(9)
F2–Fe–N3	86.86(10)	N5–Cu–O1	89.80(9)
F1–Fe–N3	87.21(9)	N4–Cu–O1	93.88(9)
O1–Fe–N3	167.12(9)	Fe–O1–Cu	126.72(10)

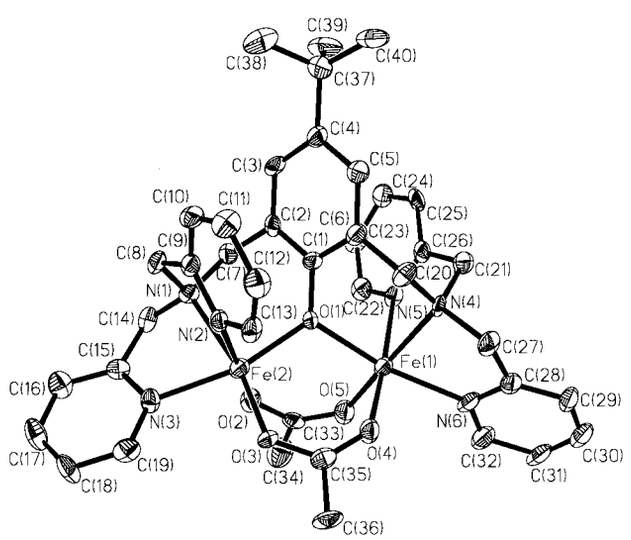

Fig. 3 The molecular arrangement of the cation in $[Fe_2(bpbp)(CH_3CO_2)_2][BF_4]_2$. Details as in Fig. 2.

distinguishing between the presence of terminal fluoride *vs.* terminal hydroxide ligands.[2] The structure of $[(bpbp)Fe(F)_2Cu(H_2O)][BF_4]_2\cdot 4H_2O$ is of significantly higher quality. Thus assignment of fluoride rather than hydroxide as the terminal ligands on the Fe^{III} is beyond doubt, thereby lending credence to our previous assignment of terminal fluoride ligands in $[(bpbp)Fe(F)_2Fe(H_2O)_2][BF_4]_2\cdot 4H_2O$.

Table 3 Selected bond lengths (Å) and angles (°) for the cation of $[Fe_2(bpbp)(CH_3CO_2)_2][BF_4]_2$

Fe1–O5	2.019(5)	Fe2–O3	1.947(5)
Fe1–O1	2.088(4)	Fe2–O1	1.951(5)
Fe1–O4	2.108(5)	Fe2–O2	1.974(5)
Fe1–N6	2.148(6)	Fe2–N3	2.152(6)
Fe1–N5	2.184(6)	Fe2–N2	2.165(6)
Fe1–N4	2.206(6)	Fe2–N1	2.200(5)
O5–Fe1–O1	97.8(2)	O3–Fe2–O2	96.0(2)
O5–Fe1–O4	94.4(2)	O1–Fe2–O2	95.0(2)
O1–Fe1–O4	89.1(2)	O3–Fe2–N3	94.2(2)
O5–Fe1–N6	99.1(2)	O1–Fe2–N3	164.6(2)
O1–Fe1–N6	162.8(2)	O2–Fe2–N3	85.5(2)
O4–Fe1–N6	86.7(2)	O3–Fe2–N2	91.0(2)
O5–Fe1–N5	91.8(2)	O1–Fe2–N2	85.2(2)
O1–Fe1–N5	84.7(2)	O2–Fe2–N2	172.8(2)
O4–Fe1–N5	171.8(2)	N3–Fe2–N2	92.5(2)
N6–Fe1–N5	97.6(2)	O3–Fe2–N1	164.4(2)
O5–Fe1–N4	168.6(2)	O1–Fe2–N1	89.6(2)
O1–Fe1–N4	87.4(2)	O2–Fe2–N1	94.4(2)
O4–Fe1–N4	95.9(2)	N3–Fe2–N1	75.0(2)
N6–Fe1–N4	76.5(2)	N2–Fe2–N1	78.4(2)
N5–Fe1–N4	78.5(2)	Fe2–O1–Fe1	113.6(2)
O3–Fe2–O1	101.0(2)		

Crystal structure of $[Fe_2(bpbp)(CH_3CO_2)_2][BF_4]_2$

Selected bond distances and angles are listed in Table 3 (see Table 1 for other crystallographic parameters). The structure of $[Fe_2(bpbp)(CH_3CO_2)_2][BF_4]_2$ (Fig. 3) shows an arrangement of the cation similar to that found for the closely related complex $[Fe_2(bpmp)(C_2H_5CO_2)_2][BPh_4]_2\cdot CH_3COCH_3\cdot 0.5CH_3CN$, bpmp = 4-methyl-2,6-bis[bis(2-pyridylmethyl)aminomethyl]-phenolate(1−).[3f] The significant differences in the Fe–O bond lengths about the two iron centres indicate that Fe1 is the iron(II) and Fe2 the iron(III) atom. The Fe···Fe distance of 3.380(2) Å is comparable to that of 3.365(1) Å found for $[Fe_2(bpmp)(C_2H_5CO_2)_2]^{2+}$,[3f] and significantly shorter than the Fe···M distances in $[(bpbp)Fe(F)_2Cu(H_2O)][BF_4]_2\cdot 4H_2O$ and $[(bpbp)Fe(F)_2Fe(H_2O)_2][BF_4]_2\cdot 4H_2O$[3] (3.828(1) and 3.819(4) Å respectively).

Electrochemistry

Cyclic voltammograms of the bis-fluoro Fe^{III}/M^{II} complexes are not as straightforward as for their bis-acetato-bridged counterparts. The latter show clearly reversible behaviour, with no apparent complicating features. However they also point strongly towards stabilization of the mixed-valence state. Voltammetric analysis of the bis-fluoro Fe^{III}/Fe^{II} complex suggests that the exogenous water and/or fluoride ligand can easily be substituted by the external solvent. This is illustrated by the CV

of $[(bpbp)Fe(F)_2Fe(H_2O)_2][BF_4]_2$ in methanol shown in Fig. 4. It is dominated by two peaks with the midpoint potentials at *ca.* 50 and *ca.* −550 mV. These match approximately the two peaks of the bis-acetato complex, and as for the latter the 600 mV peak separation reflects strong interaction between the two iron centres. The cathodic and anodic peak separations of the individual signals, however, exceed significantly 59 mV, and additional peaks are conspicuously apparent. This is indicative of the presence of more than a single species and irreversible voltammetric patterns.

By contrast to the diiron fluoride complex the heteronuclear complexes show a single reversible Fe^{III}–Fe^{II} peak. The signals are weak but differential pulse voltammetry clearly substantiates the reversible one-electron nature of the voltammetric signal, by the 95–110 mV peak half-width, and the $(1 - \sigma)/(1 + \sigma)$ dependence of the peak height, with $\sigma = \exp(nF\Delta E/2RT)$, n = number of electrons transferred, F = Faraday's number, ΔE = potential relative to the equilibrium potential, R = gas constant and T = temperature. Redox potentials obtained from differential pulse voltammetric experiments are listed in Table 4

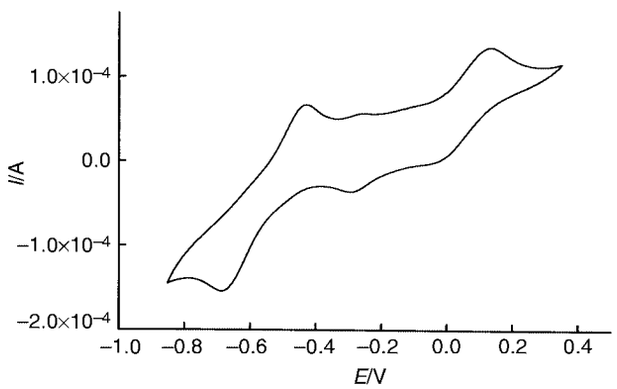

Fig. 4 The cyclic voltammogram of a 3.1×10^{-3} M solution $[(bpbp)Fe(F)_2Fe(H_2O)_2][BF_4]_2 \cdot 4H_2O$ in dry methanol. Sweep rate, 250 mV s^{-1}; reference, $Ag–AgNO_3$.

Table 4 Redox potentials for the $Fe^{III}M^{II}$–$Fe^{II}M^{II}$ couples in the difluoroaqua complexes and their bis-μ-acetato counterparts

Redox couple	Compound	$E°$/mV
$Fe^{III}Zn^{II}$–$Fe^{II}Zn^{II}$	$[(bpbp)Fe(F)_2Zn(H_2O)][BF_4]_2$	−639[a]
	$[(bpbp)FeZn(CH_3CO_2)_2][ClO_4]_2$	−334[b]
$Fe^{III}Cu^{II}$–$Fe^{II}Cu^{II}$	$[(bpbp)Fe(F)_2Cu(H_2O)][BF_4]_2$	−623[a]
	$[(bpbp)FeCu(CH_3CO_2)_2][ClO_4]_2$	−308[b]
$Fe^{III}Co^{II}$–$Fe^{II}Co^{II}$	$[(bpbp)Fe(F)_2Co(H_2O)_2][BF_4]_2$	−569[a]
	$[(bpbp)FeCo(CH_3CO_2)_2][ClO_4]_2$	−352[b]
$Fe^{III}Fe^{II}$–$Fe^{II}Fe^{II}$	$[(bpbp)Fe(F)_2Fe(H_2O)_2][BF_4]_2$	−610[a]
	$[Fe_2(bpbp)(CH_3CO_2)_2][ClO_4]_2$	−334[b]
$Fe^{III}Fe^{III}$–$Fe^{III}Fe^{II}$	$[(bpbp)Fe(F)_2Fe(H_2O)_2][BF_4]_2$	359[a]
	$[Fe_2(bpbp)(CH_3CO_2)_2][ClO_4]_2$	386[b]

[a] In 20% v/v acetone in dichloromethane *vs.* the ferrocene–ferrocenium couple. [b] From ref. 2; in acetonitrile *vs.* the ferrocene–ferrocenium couple.

which also includes the corresponding values for the $Fe^{III}M^{II}$ bis-μ-acetato-bridged analogues for comparison. The Fe^{III}–Fe^{II} couples for the iron(III) ions in the bis-fluoro complexes are lower by about 300 mV compared to those of the bis-μ-acetato-bridged complexes. This result is not unexpected given the higher concentration of negative charge around the Fe^{III} when two fluoride ions are co-ordinated. The similarity of the reduction potential for the Fe^{III}/Co^{II} complex with the other Fe^{III}/M^{II} complexes supports the proposed oxidation state distribution for the metal atoms.

Magnetochemistry

The magnetic susceptibilities of the aquafluoride complexes $[(bpbp)Fe(F)_2Fe(H_2O)_2][BF_4]_2 \cdot 4H_2O$, $[(bpbp)Fe(F)_2Co(H_2O)_2][BF_4]_2 \cdot 2.5H_2O$, $[(bpbp)Fe(F)_2Cu(H_2O)][BF_4]_2 \cdot 4H_2O$ and $[(bpbp)Fe(F)_2Zn(H_2O)][BF_4]_2 \cdot 3.5H_2O$ were recorded between 78 and 300 K. All the complexes, apart from $[(bpbp)Fe(F)_2Zn(H_2O)][BF_4]_2 \cdot 3.5H_2O$, show weak exchange coupling, antiferromagnetic in the case of the Fe^{III}/Fe^{II} and Fe^{III}/Co^{II} and ferromagnetic in the case of Fe^{III}/Cu^{II} (Table 5). For comparison Table 5 contains the magnetic coupling constants obtained for the Fe^{III}/M^{II} bis-μ-acetato-bridged analogues which were not previously reported. The Fe^{III}/Zn^{II} complexes behave as simple paramagnets with magnetic moments of 5.95–6.05 μ_B over the temperature range measured. The magnetic susceptibility measurements further support the assignment of an Fe^{III}/Co^{II} complex rather than the alternative Co^{III}/Fe^{II} assignment, by the fact that antiferromagnetic coupling is observed and can be best fitted to a high-spin iron(III) and a low-spin cobalt(II) ion. The alternative of a Co^{III}/Fe^{II} complex is excluded since a low spin diamagnetic Co^{III} is not expected to contribute to the magnetism, such that a simple high-spin iron(II) paramagnet should be observed. To our knowledge no comparable Co^{III}/Fe^{II} or Fe^{III}/Co^{II} complexes exist to which we can compare our results.

There is a notable difference in going from the singly μ-phenolato-bridged fluoride complexes to the triply μ-phenolato-bis-μ-acetato-bridged complexes in the case of Fe/Cu. Weak ferromagnetic and antiferromagnetic coupling respectively is observed. The result is consistent with the significant geometrical differences of the copper ions in $[(bpbp)Fe(F)_2Cu(H_2O)][BF_4]_2 \cdot 4H_2O$ and $[(bpbp)FeCu(CH_3CO_2)_2][ClO_4]_2 \cdot 0.5CH_3OH$. The copper ion in $[(bpbp)FeCu(CH_3CO_2)_2][ClO_4]_2 \cdot 0.5CH_3OH$ shows an octahedral geometry (confirmed by X-ray crystallography[3]), while that in $[(bpbp)Fe(F)_2Cu(H_2O)][BF_4]_2 \cdot 4H_2O$ is square pyramidal. A consequence of these geometrical differences is the orientation of the magnetic orbitals of the high spin iron(III) and the copper(II) atoms. The Cu–O1 bond is axial in the case of $[(bpbp)Fe(F)_2Cu(H_2O)][BF_4]_2 \cdot 4H_2O$ suggesting that the magnetic orbital for Cu^{II} ($d_{x^2-y^2}$) is not coplanar with any of the magnetic orbitals of Fe^{III}. Thus overlap of the magnetic orbitals of the two metal ions, *via* the hinging phenolate oxygen atom, is vanishing in $[(bpbp)Fe(F)_2Cu(H_2O)][BF_4]_2 \cdot 4H_2O$. This contrasts with the situation for the octahedral copper ion's magnetic orbital in $[(bpbp)FeCu(CH_3CO_2)_2][ClO_4]_2 \cdot 0.5CH_3OH$ which can be orientated such that overlap with the Fe^{III}-based

Table 5 Magnetic coupling constants and where possible $M–O_{phenolato}–M$ angles for the series of difluoroaqua complexes and their bis-μ-acetato-bridged $Fe^{III}M^{II}$ counterparts

	Compound	J/cm^{-1}	$M–O_{phenolato}–M$/°
$Fe^{III}Fe^{II}$	$[(bpbp)Fe(F)_2Fe(H_2O)_2][BF_4]_2 \cdot 4H_2O$	−8	124.6(3)[a]
	$[Fe_2(bpbp)(CH_3CO_2)_2][ClO_4]_2$	−4	113.6(2)
$Fe^{III}Cu^{II}$	$[(bpbp)Fe(F)_2Cu(H_2O)][BF_4]_2 \cdot 4H_2O$	+2	126.7(1)
	$[(bpbp)FeCu(CH_3CO_2)_2][ClO_4]_2$	−20	118.0(2)[a]
$Fe^{III}Co^{II}$	$[(bpbp)Fe(F)_2Co(H_2O)_2][BF_4]_2 \cdot 2.5H_2O$	−10	
	$[(bpbp)FeCo(CH_3CO_2)_2][ClO_4]_2$	−6	
$Fe^{III}Ni^{II}$	$[(bpbp)FeNi(CH_3CO_2)_2][ClO_4]_2$	−11	

[a] From ref. 2.

Table 6 Isomer shifts, δ, and quadrupole splittings, ΔE_Q, obtained from fits of the spectra shown in Figs. 5 and 6

Compound	T/K	δ/mm s^{-1}	ΔE_Q/ mm s^{-1}	δ/mm s^{-1}	ΔE_Q/ mm s^{-1}	Relative area of iron(III) component (%)
$[(bpbp)Fe(F)_2Fe(H_2O)_n][BF_4]_2$	80	0.47(1)	0.20(1)	1.17(1)	3.26(1)	52(4)
$[(bpbp)Fe(F)_2Co(H_2O)_n][BF_4]_2$	80	0.47(1)	0.21(1)	—	—	100
$[Fe_2(bpbp)(CH_3CO_2)_2][BF_4]_2$	280	0.44(4)	0.53(4)	0.98(4)	1.63(4)	52(5)
	150	0.46(4)	0.47(4)	1.10(4)	2.03(4)	49(5)
	80	0.48(2)	0.46(2)	1.13(2)	2.59(2)	49(4)

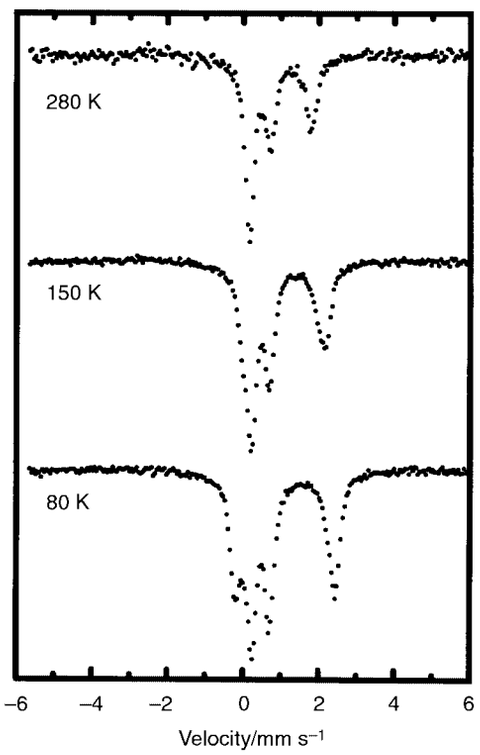

Fig. 5 The Mössbauer spectra of $[Fe_2(bpbp)(CH_3CO_2)_2][BF_4]_2$ obtained in the temperature range 80–280 K.

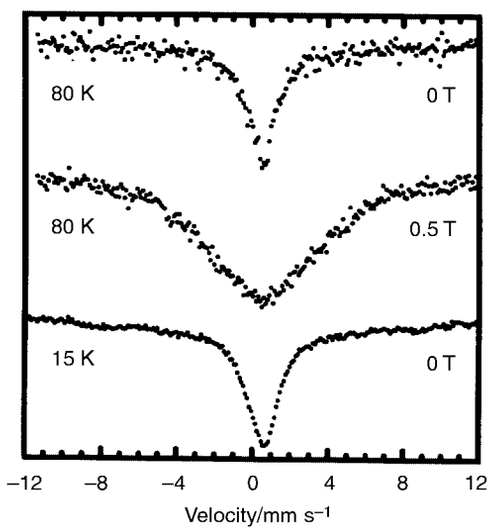

Fig. 6 The Mössbauer spectra of $[(bpbp)Fe(F)_2Cu(H_2O)][BF_4]_2\cdot 4H_2O$ obtained at 80 K without and with an applied magnetic field of 0.5 T and at 15 K without an applied field.

magnetic orbitals *via* the hinging phenolate oxygen atom is possible. With regard to the other matched pairs of singly and triply bridged complexes there is very little difference in the strength of the antiferromagnetic coupling. Within experimental error a trend is clear: acetate groups are sometimes assumed to furnish a minor contribution to magnetic exchange pathways, however the singly bridged complexes (apart from the Fe/Cu discussed above) show the largest values for J. However to counter this effect, the $F^- \cdots HOH$ moiety gives rise to a larger "bite" distance compared to an acetate bridge with the consequence of a larger M–$O_{phenolato}$–M angle (listed in Table 5). Since it is expected that the phenolate oxygen atom provides the major magnetic exchange pathway then a more obtuse M–$O_{phenolato}$–M angle will give rise to better π orbital overlap of the metal ion's magnetic orbitals *via* this oxygen atom.

Mössbauer spectroscopy

Mössbauer parameters are listed in Table 6. In accordance with the results of magnetic susceptibility and electrochemistry measurements the Mössbauer parameters of $[(bpbp)Fe(F)_2Co(H_2O)_2][BF_4]_2\cdot 2.5H_2O$ show that all of the iron atoms are in the iron(III) high spin state. The spectrum of $[(bpbp)Fe(F)_2Fe(H_2O)_2][BF_4]_2\cdot 4H_2O$ contains both iron-(II) and -(III) high spin components. The relative area of the two components is within experimental uncertainties 1:1 in accordance with an $Fe^{II}:Fe^{III}$ ratio of 1:1. Mössbauer spectra of $[Fe_2(bpbp)(CH_3CO_2)_2][BF_4]_2$ were obtained in the temperature range 80–280 K (Fig. 5) in order to determine the extent of any intramolecular electronic delocalization between the two inequivalent iron atoms. In the whole temperature range the spectra show the presence of clearly distinguishable components due to Fe^{II} and Fe^{III} in the high spin state. Thus there is no evidence for electronic delocalization like the effect seen in $[Fe_2(bpmp)(ena)_2][BF_4]_2$ (ena = deprotonated heptanoic acid).[17] The area ratio of the iron-(II) and -(III) components is very close to 1:1 and independent of temperature within experimental uncertainty. This indicates that the thermal vibrations of Fe^{II} and Fe^{III} can be described by the same effective Debye temperature. From a fit of the temperature dependence of the total spectral area an effective Debye temperature of 140 ± 10 K was obtained.

Fig. 6 shows Mössbauer spectra of $[(bpbp)Fe(F)_2Cu(H_2O)][BF_4]_2\cdot 4H_2O$ obtained at 15 K in zero applied magnetic field and at 80 K with and without an applied magnetic field of 0.5 T. The zero field spectra essentially consist of a single line with a linewidth of about 1.8 mm s^{-1}, *i.e.* almost ten times the natural linewidth indicating that the spectra are influenced by paramagnetic relaxation effects with relaxation times of the order of 1 ns.[18] An increase in the linewidth when a magnetic field is applied indicates an increase in the relaxation time. A similar effect has been observed for $Fe(NO_3)_3\cdot 9H_2O$ and explained on the basis of the crystal symmetry.[19] The space group of $[(bpbp)Fe(F)_2Cu(H_2O)][BF_4]_2\cdot 4H_2O$ is the same as that of $Fe(NO_3)_3\cdot 9H_2O$ ($P2_1/c$) and the relaxation effects can therefore be explained by the same type of mechanism.

Model complexes for fluoride-inhibited purple acid phosphatases?

It is interesting that the fluoride ligands are terminally bound at the exogenous bridging site of $[(bpbp)Fe(F)_2M(H_2O)_n]^{2+}$, since fluoride ligands bound in the terminal mode are rarer than bridging fluorides. Since a phenolate-hinged diiron complex

with Fe···Fe distance as small as 3.193(2) Å has been reported[20] (with an exogenous methoxide as bridging group) there do not appear to be geometrical contraints preventing the formation of a more usual μ-fluoride bridge rather than the aqua-fluoride-bridged compounds we have structurally characterized. This result has implications for the mode of inhibition by fluoride ions in PAPs. The M···M distances in the structures of $[(bpbp)Fe(F)_2Fe(H_2O)_2][BF_4]_2\cdot 4H_2O$ (3.726(2) Å) and $[(bpbp)Fe(F)_2Cu(H_2O)][BF_4]_2\cdot 4H_2O$ (3.828(2) Å) are significantly larger than that found in the crystal structure of red kidney bean PAP (3.26 Å)[11] without substrate or inhibitor. The two metal ions in these complexes and in red kidney bean PAP are linked by one endogenous oxygen atom, and we suggest that if F^- can substitute the isoelectronic hydroxide ion(s) proposed to be bound at the iron(III) atom in PAPs then it might bind in a terminal, rather than bridging mode, and be stabilized by hydrogen bonding to water molecules/ligands or amino acid side chains. Thus a structural motif like the Fe^{III}–$F\cdots(H_2O)M^{II}$ moieties that we have structurally characterized is pertinent.

Conclusion

The preparation of iron(III) complexes containing terminal fluoride ligands is unusual and in our hands their synthesis is possible only by exploiting the controlled decomposition of the counter anion, tetrafluoroborate. The complexes are novel mixed-metal and mixed-valence systems of an acyclic phenolate-hinged dinucleating ligand in which the exogenous site is not occupied by a bidentate bridging group. Stabilization of the terminal fluoride ligands by hydrogen bonding to adjacent water ligands and lattice water is likely to be important for their existence. The iron(III) ions of the bis-fluoride complexes are stabilized by *ca.* 300 mV towards reduction compared to the corresponding $Fe^{III}M^{II}$ bis-μ-acetato-bridged complexes. Thus the mixed-valence state for the singly bridged diiron complex is more stable that its triply bridged counterpart. X-Ray analysis shows that the "bite" distance of the $(HO–H\cdots F)^-$ group is larger that that for a bidentate carboxylate bridge with the structural consequence of an approximately 0.4 Å greater metal–metal separation for the fluoride complexes compared to their di-μ-carboxylate-bridged counterparts. With respect to the possible structural relevance of $[(bpbp)Fe(F)_2M(H_2O)_n][BF_4]_2$, M = Zn or Cu, $n = 1$; M = Co or Fe, $n = 2$, to fluoride-inhibited PAPs, we believe that if fluoride is bound at the active site then it will be bound to the iron(III) centre, and that on the basis of the present work that it is necessary to consider the hydrogen bonded structural moiety Fe–F···H–O(H)–M, M = Fe^{II} or Zn^{II}, in the case of the mammalian and plant PAPs respectively.

Acknowledgements

This work was supported by a Ph.D. grant (M. G.) and grant no. 28808 (C. J. M.) from the Danish Natural Science research council. We are grateful to Dr J. Theiner, Institut für Physikalische Chemie der Universität, Vienna, Austria for the fluoride analyses.

References

1 A. Hazell, C. J. McKenzie, B. Moubaraki and K. S. Murray, *Acta Chem. Scand.*, 1997, **51**, 470.
2 M. Ghiladi, C. J. McKenzie, A. Meier, A. K. Powell, J. Ulstrup and S. Wocadlo, *J. Chem Soc.*, *Dalton Trans*., 1997, 4011.
3 (*a*) M. Suzuki, M. Mikuriya, S. Murata, A. Uehara and H. Oshio, *Bull. Soc. Chem. Jpn*., 1987, **60**, 4305; (*b*) A. S. Borovik and L. Que, Jr., *J. Am. Chem. Soc.*, 1988, **110**, 2345; (*c*) H. Diril, H.-R. Chang, M. J. Nilges, X. Zhang, J. A. Potenza, H. J. Schugar, D. N. Hendrickson and S. S. Isied, *J. Am. Chem. Soc.*, 1988, **110**, 625; (*d*) R. M. Buchanan, K. J. Oberhausen and J. F. Richardson, *Inorg. Chem.*, 1988, **27**, 971; (*e*) H. Diril, H.-R. Chang, M. J. Nilges, X. Zhang, J. A. Potenza, H. J. Schugar, S. S. Isied and D. N. Hendrickson, *J. Am. Chem. Soc.*, 1989, **111**, 5102; (*f*) A. S. Borovik, V. Papaefthymiou, L. F. Taylor, O. P. Anderson and L. Que, Jr. *J. Am. Chem. Soc.*, 1989, **111**, 6183; (*g*) T. R. Holman, C. Juarez-Garcia, M. P. Hendrich, L. Que, Jr. and E. Münck, *J. Am. Chem. Soc.*, 1990, **112**, 7611; (*h*) M. S. Mashuta, R. J. Webb, J. K. McCusker, E. A. Schmitt, K. J. Oberhausen, J. F. Richardson, R. M. Buchanan and D. N. Hendrickson, *J. Am. Chem. Soc.*, 1992, **114**, 3815; (*i*) W. Kanda, W. Moneta, M. Bardet, E. Bernard, N. Debaecker, J. Laugier, A. Boussekou, S. Chardon-Noblat and J.-M. Latour, *Angew. Chem.*, *Int. Ed. Engl.*, 1995, **34**, 588; (*j*) A. Neves, M. A. de Brito, I. Vencato, V. Drago, K. Griesar and W. Haase, *Inorg. Chem.*, 1996, **35**, 2360.
4 K. Anzai, K. Hatano, Y. J. Lee and W. R. Scheidt, *Inorg. Chem.*, 1981, **20**, 2337; W. R. Scheidt, Y. J. Lee, S. Tamai and K. Hatano, *J. Am. Chem. Soc.*, 1983, **105**, 778; S. C. Lee and R. H. Holm, *Inorg. Chem.*, 1993, **32**, 4745; S. Christie, S. Subramanian, L. Wang and M. J. Zaworotko, *Inorg. Chem.*, 1993, **32**, 5415.
5 P. Glavic, J. Slivnik and A. Bole, *J. Inorg. Nucl. Chem.*, 1979, **41**, 248; K. C. Patil and E. A. Secco, *Can. J. Chem.*, 1972, **50**, 567.
6 T. R. Musgrave and T. S. Linn, *J. Coord. Chem.*, 1973, **2**, 323.
7 J. Reedijk, J. C. Jansen, H. van Koningsveld and C. G. van Kralingen, *Inorg. Chem.*, 1978, **17**, 1990; R. W. M. ten Hoedt, J. Reedijk and G. C. Verschoor, *Recl. Trav. Chim. Pays-Bas*, 1981, **100**, 400; W. C. Velthuizen, J. G. Haasnoot, A. J. Kinneging, F. J. Rietmeijer and J. Reedijk, *J. Chem. Soc.*, *Chem. Commun.*, 1983, 1366; F. J. Rietmeijer, R. A. G. de Graaff and J. Reedijk, *Inorg. Chem.*, 1984, **23**, 151; J. Verbiest, J. A. C. van Ooijen and J. Reedijk, *J. Inorg. Nucl. Chem.*, 1980, **42**, 971; J. Reedijk, *Comments Inorg. Chem.*, 1982, **1**, 379; W. Vreugdenhil, P. J. M. W. L. Birker, R. W. M. ten Hoedt, G. C. Verschoor and J. Reedijk, *J. Chem. Soc.*, *Dalton Trans.*, 1984, 429; J. Reedijk and R. W. M. ten Hoedt, *Recl. Trav. Chim. Pays-Bas*, 1982, **101**, 49.
8 J. B. Vincent, M. W. Crowder and B. A. Averill, *Biochemistry*, 1991, **30**, 3025; M. W. Crowder, J. B. Vincent and B. A. Averill, *Biochemistry*, 1992, **31**, 9603.
9 T. Klabunde, N. Sträter, R. Frölich, H. Witzel and B. Krebs, *J. Mol. Biol.*, 1996, **259**, 737.
10 E. Pedersen, *Acta Chem. Scand.*, 1972, **26**, 333; J. Josephsen and E. Pedersen, *Inorg. Chem.*, 1977, **16**, 2534.
11 C. J. O'Connor, *Prog. Inorg. Chem.*, 1982, **29**, 203.
12 J. Cosier and A. M. Glazer, *J. Appl. Crystallogr.*, 1986, **19**, 105.
13 Siemans SMART and SAINT, Area-Detector Control and Integration Software, Siemens Analytical X-Ray Instruments Inc., Madison, WI, 1995; G. M. Sheldrick, SADABS, Program for Absorption Correction, Siemens Analytical X-Ray Instruments Inc., Madison, WI, 1996.
14 G. M. Sheldrick, SHELXTL 95, Siemens Analytical X-Ray Instruments Inc., Madison, WI, 1995.
15 A. L. Spek, *Acta Crystallogr.*, *Sect. A*, 1990, **46**, C-34.
16 A. Hazell, K. B. Jensen, C. J. McKenzie and H. Toftlund, *Inorg. Chem.*, 1994, **33**, 3127.
17 Y. Maeda, Y. Tanigawa, N. Matsumoto, H. Oshio, M. Suzuki and Y. Takashima, *Bull. Soc. Chem. Soc. Jpn.*, 1994, **67**, 125; T. Manago, S. Hayami, H. Oshio, S. Osaki, H. Hasuyama, R. H. Herber and Y. Maeda, *J. Chem. Soc.*, *Dalton Trans.*, 1999, 1001.
18 S. Mørup, *Mössbauer Effect Methodology*, eds. I. J. Gruverman C. W. Seidel and D. K. Dieterly, Plenum, New York, 1974, vol. 9, p. 127; *Paramagnetic and Superparamagnetic Relaxation Phenomena Studied by Mössbauer Spectroscopy*, Polyteknisk Forlag, Lyngby, 1981.
19 S. Mørup and N. Thrane, *Chem. Phys. Lett.*, 1973, **21**, 363; S. Mørup, *J. Phys. Chem. Solids*, 1974, **35**, 1159; S. Mørup, F. Sontheimer, G. Ritter and R. Zimmermann, *J. Phys. Chem. Solids*, 1978, **39**, 123.
20 C. Belle, I. Gautier-Luneau, J.-L. Pierre, C. Scheer and E. Saint-Aman, *Inorg. Chem.*, 1996, **35**, 3706.

Paper 9/02678I